DOI: 10.1002/ejic.200700210

Synthesis of Carbon and Silica Hollow Spheres with Mesoporous Shells using Polyethylene Oxide/Phenol Formaldehyde Polymer Blend

Chun-Yi Chang-Chien,[a] Chun-Han Hsu,[a] Tsung-Ying Lee,[a] Che-Wei Liu,[a] Sheng-Ho Wu,[a] Hong-Ping Lin,*[a,b] Chih-Yuan Tang,[c] and Chin-Yen Lin[c]

Keywords: Polymer blends / Mesoporous materials / Metal oxides / Organic templates

Polyethylene oxide/phenol formaldehyde silica composite hollow spheres were obtained from a fast silicification of a polymer blend, containing polyethylene oxide (PEO) as silica gelator and phenol formaldehyde (PF) polymer as carbon source, in a highly diluted silica solution at pH ≈ 5.0–6.0. The PF–PEO/silica hollow spheres can be feasibly converted to mesoporous silica hollow spheres by hydrothermal treatment and calcination, and to mesoporous carbon hollow spheres after pyrolysis under a nitrogen atmosphere and silica etching. Because the formation of the hollow spheres is kinetically controlled, the diameter of the hollow spheres is dependent on the molecular weight of the PEO polymer, pH value of the silica solution, and the PF content, and the size can be tuned within a range of a few micrometers to tens of nanometers. These mesoporous hollow spheres have high surface areas and large pore sizes and volumes. In practice, the mesoporous carbon hollow spheres with an interconnected mesostructure were used as a solid template to prepare different metal oxide hollow spheres. After impregnation of the proper metal oxide precursors and calcination, the γ-Al_2O_3, *anatase*-TiO_2, α-Fe_2O_3, ZrO_2, MgO, and CeO_2 hollow spheres composed of nanoparticles were readily synthesize.

Introduction

Since the discovery of mesoporous silicas by Mobil researchers and Kuroda,[1] the construction of organic templates to synthesize advanced materials has become a significant area of scientific and technological interest.[2,3] Because of potential applications in drug storage and release, confined-space catalysis, thermal and electrical insulators, separation, and biomolecule release, the fabrication of functional porous materials with hollow interiors has attracted much attention.[4–10] Typically, hollow spheres of various diameters and wall thicknesses were synthesized by using polymer or silica beads,[5,6] gold nanoparticles,[7] emulsion drops,[8–9] or multi-layers vesicles[10] as interior templates. However, a removable expensive polymer bead, silica, or a Au nanoparticle is energy-consuming and uneconomic. Moreover, fine tuning for the chemical composites and synthetic conditions (i.e. temperature, stirring rate, pH value, etc.) to prepare stable emulsions or vesicles as the morphological templates of the inorganic materials is a sophisticated approach. In addition to creating the hollow interior, introduction of porosity to the shell is also crucially important for controlling accessibility and permeability of the void interior space to the environment.[11] Up to now, the development of a convenient synthetic method and the use of cost-effective precursors to generate the materials with hollow interiors and porous shell is still of much interest.

In polymer chemistry,[12] it is well-known that thermosetting phenol formaldehyde polymers (PF) have been widely used as carbon precursors in industry and that nature-friendly polyethylene oxide (PEO) homopolymers have a high affinity to aggregate with silica species through hydrogen bonding between the ether and silanol groups. From analysis of the molecular structures of the PEO polymer and PF polymers, it can be seen that the ether groups (i.e. –O– : hydrogen-bonding acceptor) of the PEO polymers and the methylene hydroxide and phenol groups (i.e. $–CH_2OH$ and $C_6H_6–OH$: hydrogen-bonding donor) of the PF polymers have a high degree of hydrogen-bonding complementarity. Therefore, PEO and PF polymers could construct a homogeneously miscible PF–PEO polymer blend. On the basis of these concepts, in this study we used the PF–PEO polymer blend in a water/ethanol solution as the morphological and mesostructural template of the silica. When combined with a stock sodium silicate solution at pH ≈ 5.0–6.0, PF–PEO/silica hollow spheres were quickly generated. Because the synergistic PF–PEO/silica hollow spheres contain carbonizable PF polymer and silica, hollow

[a] Department of Chemistry, National Cheng Kung University, Tainan, 701, Taiwan
E-mail: hplin@mail.ncku.edu.tw
[b] Research and Education Division Center for Micro/Nanoscience and Technology, National Cheng Kung University, Tainan, 701, Taiwan
[c] Precision Instrument Center, National Taiwan University, Taipei, 106, Taiwan

Supporting information for this article is available on the WWW under http://www.eurjic.org or from the author.

carbon spheres with mesoporous shells were prepared after pyrolysis and silica removal. Alternatively, hollow silica spheres with porous shells were obtained from hydrothermal treatment and calcination in air.

Results and Discussion

Figure 1 shows the representative SEM image of the as-synthesized PF–PEO6000/silica composite. It can be clearly seen that the morphology of the particle is spherical and that the diameter of the sphere ranges from 1.0 to 0.5 μm. Some broken spheres reveal that the spheres are hollow and the wall thickness is around 0.1–0.2 μm. The inner cavities of the spheres were clearly identified by TEM contrast imaging (Figure 1B). Clearly, the spheres are almost hollow (>90%). The TGA curve of the PF–PEO6000/silica composite is intermediate between the TGA curves of the PEO/silica and PF polymer (Figure 1C), which demonstrates a homogeneous blending between PEO6000 and PF polymers. This average in combustion temperature occurs commonly in homogeneous organic or polymer blends.

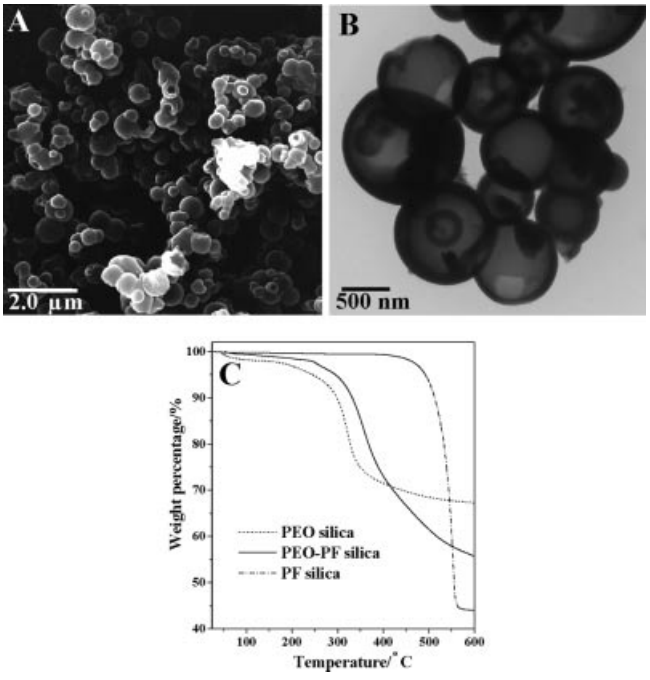

Figure 1. SEM (A) and TEM (B) images of the PF–PEO6000/silica hollow spheres prepared by using a synthetic component of PF/PEO6000/sodium silicate/H_2O = 2.0: 2.0: 8.0: 315.0 g. (C). TGA curves of the PEO6000/silica, PF–PEO/silica, and PF/silica composites.

Because the PF–PEO/silica composite hollow spheres contain the carbonizable PF polymer, the mesoporous carbon hollow spheres can thus be easily obtained from high-temperature pyrolysis and silica removal by HF etching. The resulting mesoporous carbon retains the spherical morphology (Figure 2A). Some broken or folded hollow spheres reveal that the mesoporous carbon spheres are hollow.[13] The hollow interiors of the carbon spheres can be more clearly shown in a TEM image (Figure 2B). The shell thickness of the hollow mesoporous carbon spheres is around 0.1 μm. The preservation of the hollow-sphere morphology indicates that the thermosetting PF polymers disperse homogeneously within the shell, and then form a stable cross-linked framework to keep the hollow-sphere morphology. The high-magnification TEM image clearly shows that the mesostructure of the hollow sphere's shell is wormhole-like (i.e. interconnected), and the pore size is around a few nanometers (inset of Figure 2B). In parallel to the TEM observations, the hollow mesoporous carbon spheres exhibit a type IV N_2 adsorption–desorption isotherm with a capillary condensation occurring at P/P_0 = 0.3 to 0.4 (Figure 2C). By analyzing the adsorption isotherm, the mesoporous carbon hollow spheres have a high Brunauer–Emmett–Teller surface area (≈1500 $m^2 g^{-1}$), large Barrett–Joyner–Halenda pore size (≈2.6 nm), and pore volume (≈0.93 $cm^3 g^{-1}$), as do the mesoporous carbons obtained from the mesoporous silica-templating method.[4]

To obtain information about the thermal stability and carbon phase of the hollow mesoporous carbon spheres, TGA, Raman spectroscopy, and XRD investigations were performed.[14,15] The hollow mesoporous carbon spheres exhibit significant weight loss in a narrow temperature range between 600 and 650 °C (Supporting Information, Figure S1). Thus, the porous carbon of high thermal stability can be easily produced from the PF–PEO6000/silica composite. The silica residue in the porous carbon is less than 2.0 wt.-%, indicating that the silica was almost entirely removed by HF etching. The mesoporous carbon hollow spheres show two broad XRD peaks that can be indexed to (002) and (100) diffraction peaks for the amorphous carbons (Figure 2D). In addition, the Raman spectrum of the sample displays two broad vibration bands (inset of Figure 2D). One band is around 1580 cm^{-1} (G-band; the interplane sp^2 C–C stretching) and the other band is located around 1340 cm^{-1} (D-band; the defects within the carbon), which also indicate the amorphous carbon structure.[16]

In addition to producing mesoporous carbon hollow spheres, mesoporous silica hollow spheres also can be generated from the PF–PEO6000/silica composite after hydrothermal treatment at 100 °C and calcination at 560 °C in air. The microtome TEM image shows that the mesostructure of the shell of the hollow silica spheres is disordered and that the pore size is around a few nanometers (Figure 2E). Therefore, the mesoporous silica hollow sphere displays type IV N_2 adsorption–desorption isotherms with an apparent capillary condensation occurring at P/P_0 = 0.6–0.7 (Figure 2F). The mesoporous silica hollow spheres have Brunauer–Emmett–Teller surface area of 520 $m^2 g^{-1}$, a mean Barrett–Joyner–Halenda pore size of 6.2 nm, and a pore volume of 0.75 $cm^3 g^{-1}$. Consequently, the high-quality mesoporous carbon and silica hollow spheres can be conveniently obtained from the calcination and (carbonization + silica removal) of the PF–PEO/silica composite hollow spheres, respectively.

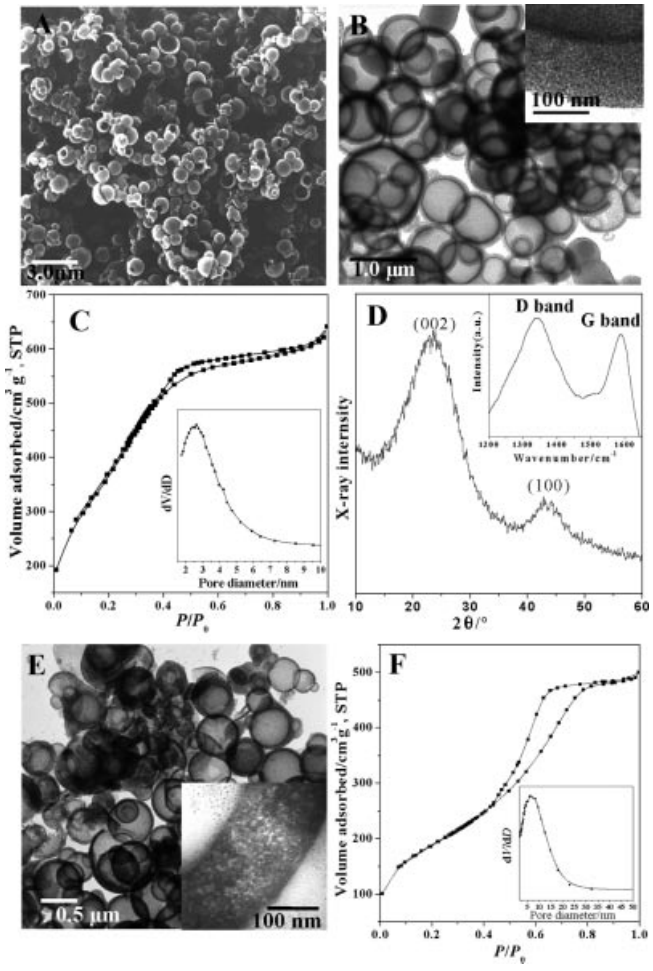

Figure 2. SEM (A) and TEM (B) micrographs of the mesoporous carbon hollow spheres. Inset is HR-TEM image of mesoporous shell of the mesoporous carbon hollow spheres. (C). N_2 adsorption–desorption isotherm of the mesoporous carbon hollow spheres. Inset is the BJH pore size distribution. (D) High-angle XRD pattern of the mesoporous carbon hollow spheres. Inset is the Raman spectrum. (E). TEM image of the mesoporous silica hollow spheres. Inset is the microtome TEM image. (F) N_2 adsorption–desorption isotherm of the mesoporous silica hollow spheres. Inset is the BJH pore-size distribution.

When using other PEO homopolymers of different molecular weights to blend with the same amount of PF polymer, the TEM images revealed that the prepared mesoporous carbon samples consisted of hollow spheres (yield > 90%) with different diameters (Figure 3). By comparing the diameters of these mesoporous carbon hollow spheres, it is clear that the average diameters and the shell thickness decrease with an increase in the PEO polymer molecular weight. According to these current results, the use of the PEO100000 or PEO300000 polymers gave hollow spheres in tens of nanometers (Figure 3B, C), and submicro- to micrometer hollow sphere were obtained with PEO10000 or PEO6000 (Figures 3A and 2B). Like the hollow mesoporous carbon spheres synthesized with PEO6000, other hollow mesoporous carbon spheres have high surface area, mesoporosity, and large pore volume (Supporting Information, Figure S2). Clearly, the mesoporous silica hollow spheres with various diameters (tens of nanometers to micrometers) were also obtained from the hydrothermal treatment and organic template removal (Supporting Information, Figure S3). To the best of our knowledge, this is the first time that the mesoporous carbon and silica hollow spheres with various diameters have been synthesize by using the commercially attractive PF–PEO polymer blend and sodium silicate.

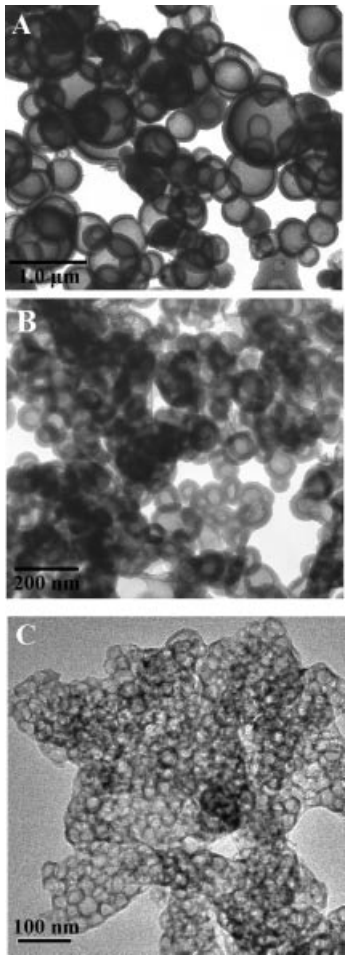

Figure 3. TEM images of the mesoporous carbon hollow spheres synthesized with PF–PEO*n* polymer blend as template. (A) n = 10000; (B) n = 100000; (C) n = 300000. The synthetic compositions are: PF/PEO*n*/sodium silicate/H_2O = 2.0: 2.0: 8.0: 315.0 g.

To understand the driving force of the formation of the hollow spheres, we poured the ethanol/water solution of the PF–PEO polymer blend into water and found that an opaque solution (i.e. PF–PEO emulsion solution) was formed at the beginning and then the hydrophobic PF polymers gradually underwent phase separation and precipitation from the aqueous phase. In contrast, when the PF–PEO polymer blend solution was added to a sodium silicate solution, a light yellow gel solution was formed in a few seconds without phase-separation and precipitation of the free PF polymers. This is because the silicate species can quickly assemble with the PEO parts in the PF–PEO polymer blend at pH around 5.0–6.0 to solidify the hydrother-

mally unstable PF–PEO emulsions and prohibit the self-precipitation of the hydrophobic PF polymer. Although the phase-separation approach is typically used to prepare hollow latex particles,[15] this is the first time that it was employed to synthesize porous materials.

On the basis of all the above observations, a simple plausible mechanism was proposed addressing the formation of the hollow spheres. As shown in Scheme 1, when the PF–PEO solution was added into a highly diluted sodium silicate aqueous solution, the hydrophobic PF polymers induced the formation of PF–PEO emulsions. At the same time, the silica species, which assemble with the PEO polymers, attach onto the outer surface of the PF–PEO emulsions. After fast further silica condensation, the PF–PEO emulsions were solidified prior to the PF phase-separation, and then the hollow PF–PEO/silica hollow spheres were generated. Therefore, with careful control of the condensation rate of the silica species on the PF–PEO emulsions and the coalescence rate of the PF–PEO emulsions induced by the hydrophobic PF polymer, a capsule-shaped PF–PEO/silica composite was obtained. Because the PEO homopolymer of higher molecular weight can assemble faster with the silica species than the lower molecular weight polymers, the average diameter of the trapped PF–PEO/silica hollow spheres becomes smaller (Figure 3).

According to silica chemistry, it is well-known that the silica condensation rate depends on the pH value.[17] Figure 4 exhibits the mesoporous carbon samples prepared at different pH values. It is clear that the pH value of the silicate solution must be tuned in the range of 5.0–6.0 to get the hollow spheres, where matching interaction between PEO and silica species (i.e. hydrogen bonding between $-CH_2CH_2O^{\delta-}$ of the PEO polymer and the silanol group –SiOH of the silica species) and fast silica condensation rate could prevent the self-precipitation of the PF polymers.[18] In this pH value range, the silica condensation rate increases with the pH value,[17] and thus the average diameter of the hollow spheres decreases as the pH value increases (Figures 2B, 4B, and 4D). However, outside of this pH range, the hollow spheres were no longer obtained. At pH values <5.0, the slow silica condensation rate led to the generation of micrometer-sized solid spheres or particles (Figure 4A). However, at pH values >7.0, mismatching interactions between the negatively charged silicate species and the partially negative PEO polymer resulted in the separation of the silica and the PF–PEO polymer blend, which led to the precipitation of the PF polymers.

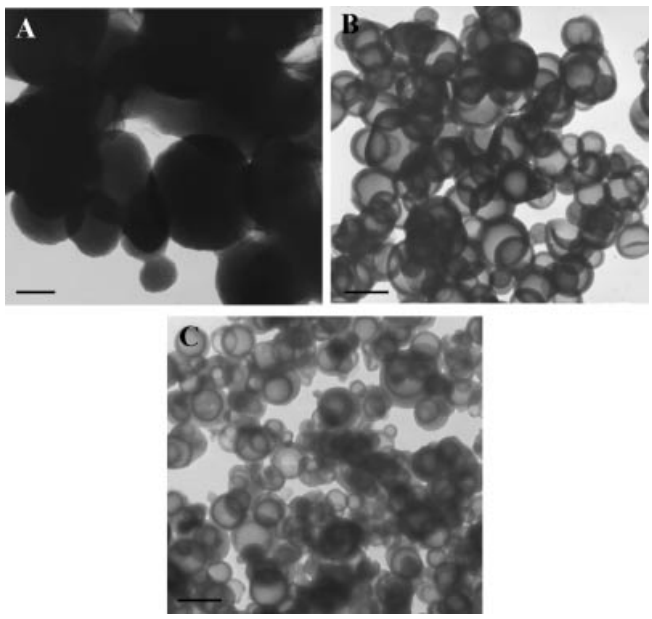

Figure 4. TEM micrographs of the mesoporous carbon hollow spheres synthesized in silica solutions at different pH value (PF/PEO6000 weight ratio = 2.0). (A) pH = 4.0; (B) pH = 5.5; (C) pH = 6.0. Scale bar = 500 nm.

In addition to studying the effect of the silica condensation rate on the diameter of the hollow spheres, we also changed the content of the PF polymer to control the coalescence rate of the PF–PEO emulsions. As expected, we found that the average diameter of the mesoporous carbon hollow spheres increased with an increase in the PF polymer content (Figure 5). When the PF/PEO6000 weight ratio is higher than 1.5, the PF polymer precipitation rate is relatively too fast to be completely trapped and some PF polymer precipitates. Moreover, it must be mentioned that the yield of the carbon is determined by the PF content. At low PF/PEO6000 weight ratios (<0.5), the carbon yield is very low. Consequently, the appropriate PF/PEO6000 weight ratio to obtain carbon hollow spheres in a suitable yield ranges form 0.8 to 1.5. To reduce the dispersion in the diameter of the hollow spheres, considerably kinetic and thermodynamic principles behind the formation of the hollow spheres will be further studied.

It is known that there are advantages to use mesoporous carbon as solid templates:[4,19–21] (1) The high stability of the carbon framework can stand for cruel synthetic conditions. (2) The amorphous carbon should be easily removed

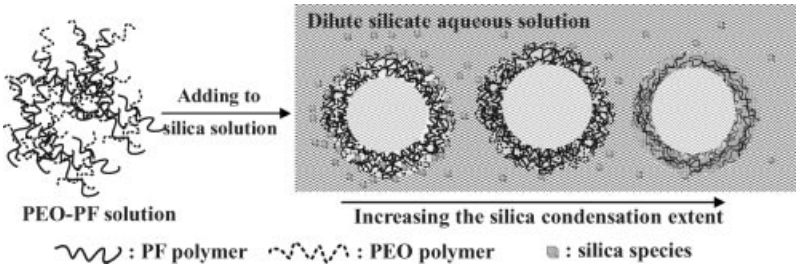

Scheme 1. Formation mechanism of the PF–PEO/silica composite hollow spheres in a highly diluted silica solution.

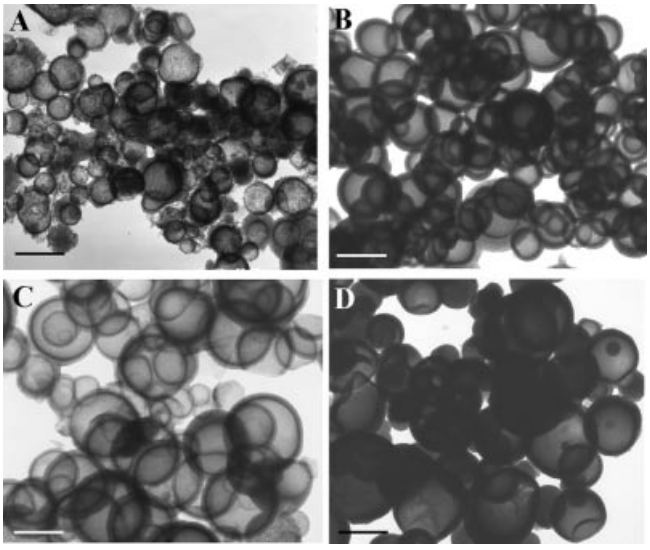

Figure 5. TEM images of the mesoporous carbon hollow spheres prepared with different PF/PEO300000 weight ratios (r) at pH = 5.0. (A) r = 0.5; (B) r = 0.8; (C) r = 1.3; (D) r = 1.5. Scale bar = 500 nm.

by calcination at temperatures higher than 600 °C. (3) Crystallization of the metal oxide can be readily achieved under the confinement of the mesostructure of carbon. In practice, we used the mesoporous carbon hollow spheres of interconnected mesostructure as a solid *exo* template to prepare the porous metal oxide hollow spheres.[22] Figure 6 shows the representative TEM and SEM images of the ZrO_2, Al_2O_3, TiO_2, and Fe_2O_3 hollow spheres prepared by impregnating mesoporous carbon hollow spheres with acidic ethanolic solutions of $Zr(OAc)_4$, $Al(NO_3)_3$, $Ti(OBu)_4$, and $Fe(NO_3)_3$ salts, respectively, and calcination at 600 °C in air. These images clearly demonstrate that the metal oxide hollow spheres can be easily obtained from a typical impregnation process by using mesoporous carbon hollow spheres as a solid template. In addition to preserving the hollow-sphere morphology, the HR-TEM image reveals that the shell of the metal oxide hollow spheres is composed of many nanocrystals (ca. 5–30 nm, insets of Figure 6). In combination with the high-angle XRD patterns of the metal oxide hollow spheres, all broad XRD peaks can be assigned undisputedly to the γ-Al_2O_3, *anatase*-TiO_2, α-Fe_2O_3, and ZrO_2 nanoparticles. According to these results, we proposed a possible mechanism for the formation of the mesoporous metal oxide hollow spheres. In the first stage, the precursors of the metal oxides can be incorporated into the interconnected nanopores of the mesoporous carbon shell. Upon heat treatment, the precursors thermally decompose, and the nanoparticles derived therefrom grow larger and crystallize. In the presence of thermally stable carbon, the crystalline dimension is confined to the nanoscale. Because the nanocrystals interlink with each other and form continuous and stable frameworks, the hollow-sphere morphology is fully replicated even after the removal of the carbon template by further high temperature heat treatment. These metal oxide hollow spheres have a high surface area (100–150 $m^2 g^{-1}$), large pore size (8.0–12.0 nm), and a large volume (0.25–0.35 $cm^3 g^{-1}$; Supporting Information, Figure S4, Table S1). In addition to ZrO_2, γ-Al_2O_3, *anatase*-TiO_2, and α-Fe_2O_3 mesoporous hollow spheres,[23–27] other metal oxide hollow spheres (e.g. MgO and CeO_2; Supporting Information, Figure S5) were also produced by using the mesoporous carbon hollow spheres as a solid template. Moreover, to obtain magnetic nanoparticles containing mesoporous carbon hollow spheres, the $Fe(NO_3)_3$ impregnated mesoporous carbon was heated to 900 °C under a N_2 atmosphere instead. Figure 6F shows that the Fe nanoparticles are embedded within the mesoporous carbon shell or in the interior of the hollow spheres. The magnetic nanoparticles containing mesoporous carbon hollow spheres demonstrate the magnetic properties (Supporting Information, Figure S6).

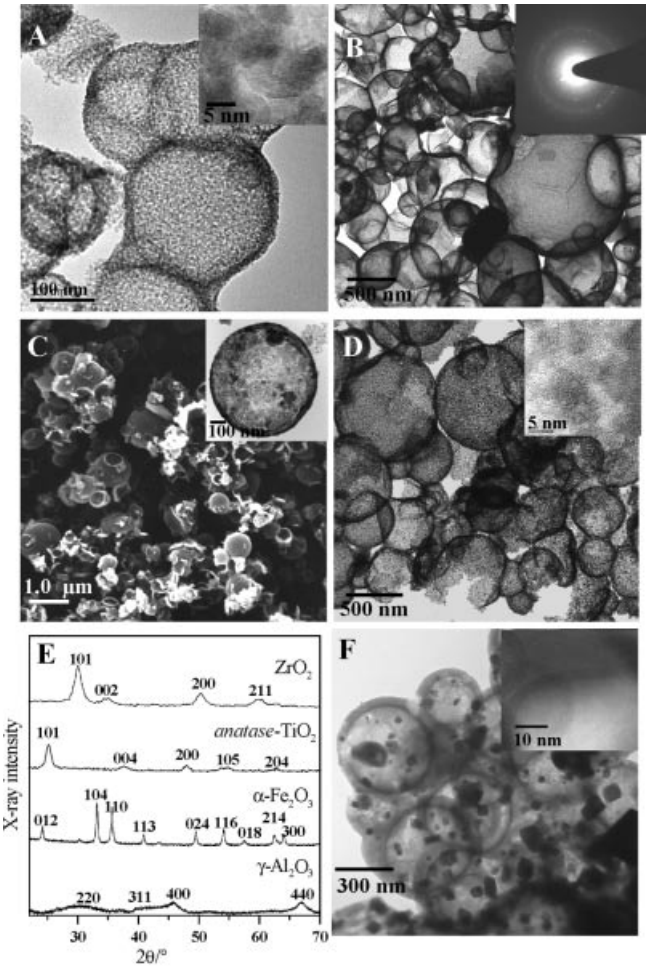

Figure 6. TEM and SEM images and XRD patterns of the mesoporous metal oxide hollow spheres prepared by using mesoporous carbon hollow spheres as hard templates. (A) ZrO_2; (B) γ-Al_2O_3; (C) α-Fe_2O_3; (D) *anatase*-TiO_2, (E) XRD patterns; (F) The Fe nanoparticle containing mesoporous carbon hollow spheres obtained from pyrolysis of a $Fe(NO_3)_3$ impregnated mesoporous carbon hollow spheres at 700 °C under an atmosphere of N_2. Insets are the HR-TEM and electron-diffraction images of the metal oxides and iron nanoparticles.

Conclusions

In brief, we have described a new method to conveniently synthesize PF–PEO/silica hollow spheres. The synergistic PF–PEO/silica hybrid composite can be transferred to mesoporous carbon and mesoporous silica hollow spheres as required. This synthetic method for the preparation of hollow spheres with different diameters involves the simple mixing of well-defined precursors and changing the components and pH value of the mixture; thus scale-up of the hollow spheres is readily accomplished. The phase-separation approach can be extended to different polymer blends and nonsilica metal oxides. With good control of assembling kinetics, one can judiciously select other polymer blends to manufacture hollow mesoporous spheres with high flexibility in their compositions. In addition, the use of stable mesoporous carbon hollow spheres is an alternative for the preparation of metal oxides hollow spheres of high crystallinity and magnetic mesoporous carbon hollow spheres. These hollow spheres of high composition-flexibility have potential to be applied as a catalyst, absorbent, sensor, magnetically separable carrier, microcapsule, supercapacitor, and as an aid in drug-delivery and fuel cells.

Experimental Section

Typical Synthesis of Mesoporous Carbon and Silica Hollow Spheres: The PEO (Acrös) (2.0 g) and PF (0.5–3.0 g; PF2180, phenol/aldehyde, 0.8–0.9; MW ca. 96000; Chung-Chun Plastic, Taiwan) polymers were dissolved in a mixture of ethanol (20.0 g) and water (5–15 g) to form a clear solution. Then, the PF–PEO blend solution was poured quickly into an acidified sodium silicate solution aqueous solution (pH ≈ 5.0–6.0) at 40 °C, which was prepared by adjusting the pH value of a mixture of sodium silicate (27 wt.-% SiO_2, 8.0 g, Aldrich) and water (300.0 g) to 4.0–7.0 and aging for 3–10 min. A light-yellowed precipitate formed within a few seconds. Filtration, washing, and drying at 100 °C gave the PF–PEO/silica hollow spheres. The mesoporous carbon hollow spheres with mesoporous shells were gained after a pyrolysis at 1000 °C under a N_2 atmosphere for 2 h and silica removal by 6 wt.-% HF etching. Alternatively, to obtain the hollow silica spheres with a mesoporous shell, the PF–PEO/silica hollow spheres were kept static in a polypropylene bottle at 100 °C for 1 d and calcined at 580 °C for 6 h to remove the organic template.

Synthesis of Metal Oxides Hollow Sphere: A proper amount of metal oxide precursor (metal/carbon ≈ 1:50 in mol) was dissolved in an acidic ethanolic solution (95 wt.-% ethanol, 20.0 g, conc. HNO_3, 1.0 g). The $Zr(OAc)_4$, $Al(NO_3)_3$, $Ti(OBu)_4$, and $Fe(NO_3)_3$ were used as the precursors to the ZrO_2, γ-Al_2O_3, *anatase*-TiO_2, and α-Fe_2O_3 hollow spheres, respectively. Then, the ethanolic solution was combined with the mesoporous carbon hollow sphere sample (0.4 g). After stirring for 1 d under ambient conditions and dried at 60 °C to evaporate the solvent, the dried metal oxide precursor impregnated mesoporous carbon was obtained. Calcination at 600 °C for 8 h to remove the mesoporous carbon template gave the metal oxides hollow spheres.

Characterization: N_2 adsorption–desorption isotherms were obtained at 77 K with a Micromeritics ASAP 2010 apparatus. Before analysis, the sample was degassed at 120 °C for about 6 h at 10^{-3} Torr. The pore size distribution was obtained from the analysis of the adsorption branch by using the BJH (Barrett–Joyner–Halenda) method. Scanning electron microscopy (SEM) and transmission electron microscopy (TEM) images were obtained with an S-800 (Hitachi) operated at an acceleration voltage of 20 keV and an H-7500 (Hitachi) operated at 100 keV, respectively. The organic content in the mesoporous silicas and the porous carbon thermostability were measured by thermogravimetric analysis (TGA). TGA tests were conducted with a TA Q-50 thermogravimetric system. In a typical experiment, ca. 10 mg of the sample was heated to 700–800 °C at 10 °C min^{-1} in air. Raman spectra were obtained with a Dilor XY Raman spectrum, using an Ar laser with an excitation wavelength of 514.5 nm.

Supporting Information (see footnote on the first page of this article): TGA curve of the mesoporous carbon hollow spheres, N_2 adsorption–desorption isotherm of the PF–PEO*n* polymer blend-templated mesoporous carbon hollow spheres, SEM images of the different PF–PEO*n* polymer blend templated mesoporous silica hollow spheres, N_2 adsorption–desorption isotherms of the different mesoporous metal oxides hollow spheres, TEM images of mesoporous MgO and CeO_2 hollow spheres, photograph showing magnetic Fe@mesoporous carbon hollow sphere, and table of the precursors and properties of the metal oxides and Fe@carbon hollow spheres.

Acknowledgments

Authors thank Pann Asia Chemical Corporation and Chung-Chun Plastic, Taiwan for providing the PEO and PF polymers. This research is financially supported by the National Science Council of Taiwan (NSC95-2113-M-006-011-MY3, NSC95-2120-M-006-009, and NSC95-2323-B-006-008).

[1] a) T. Yanagisawa, T. Shimizu, K. Kuroda, C. Kato, *Bull. Chem. Soc. Jpn.* **1990**, *63*, 988–992; b) C. T. Kresge, M. E. Leonowicz, W. J. Roth, J. C. Vartuli, J. S. Beck, *Nature* **1992**, *359*, 710–712.
[2] a) D. Zhao, J. Feng, Q. Huo, N. Melosh, G. H. Fredrickson, B. F. Chmelka, G. D. Stucky, *Science* **1998**, *279*, 548–552; b) J. Y. Ying, C. P. Mehnert, M. S. Wong, *Angew. Chem. Int. Ed.* **1999**, *38*, 56–77.
[3] a) P. T. Tanev, M. Chibwe, T. J. Pinnavaia, *Nature* **1994**, *368*, 321–323; b) P. T. Tanev, T. J. Pinnavaia, *Science* **1995**, *267*, 865–867.
[4] a) J. Lee, J. Kim, T. Hyeon, *Adv. Mater.* **2006**, *18*, 2073–2094; b) S. B. Yoon, K. Sohn, J. Y. Kim, C.-H. Shin, J.-S. Yu, T. Hyeon, *Adv. Mater.* **2002**, *14*, 19–21.
[5] a) Z. Zhong, Y. Yin, B. Gates, Y. Xia, *Adv. Mater.* **2000**, *12*, 206–209; b) S. W. Kim, M. Kim, W. Y. Lee, T. Hyeon, *J. Am. Chem. Soc.* **2002**, *124*, 7642–7643.
[6] a) F. Caruso, R. A. Caruso, H. Mohwald, *Science* **1998**, *282*, 1111–1114; b) M. Yang, J. Ma, C. Zhang, Z. Yang, Y. Lu, *Angew. Chem. Int. Ed.* **2005**, *44*, 6727–6730.
[7] a) X. Zheng, C. Liu, Y. Xie, *Eur. J. Inorg. Chem.* **2006**, 2364–2369; b) N. Singh, L. A. Lyon, *Chem. Mater.* **2007**, *19*, 719–726.
[8] a) C. I. Zoldesi, A. Imhof, *Adv. Mater.* **2005**, *17*, 924–928; b) D. Walsh, B. Lebeau, S. Mann, *Adv. Mater.* **1999**, *11*, 324–328.
[9] a) X. W. Lou, Y. Wang, C. Yuan, J. Y. Lee, L. A. Archer, *Adv. Mater.* **2006**, *18*, 2325–2329; b) R. K. Rana, V. S. Murthy, J. Yu, M. S. Wang, *Adv. Mater.* **2005**, *17*, 1145–1150.
[10] a) Y. Q. Yeh, B. C. Chen, H. P. Lin, C. Y. Tang, *Langmuir* **2006**, *22*, 6–9; b) H. P. Lin, C. Y. Mou, *Acc. Chem. Res.* **2002**, *35*, 927–935.
[11] a) H.-P. Hentze, S. R. Raghavan, C. A. McKelvey, E. W. Kaler, *Langmuir* **2003**, *19*, 1069–1074; b) D. H. Hubert, W. M. Jung, P. M. Frederik, P. H. H. Bomans, J. Meuldijk, A. L. German, *Adv. Mater.* **2000**, *12*, 1286–1290.

[12] M. P. Stevens, *Polymer Chemistry*, Oxford University, Oxford, New York, **1999**.
[13] P. M. Arnal, F. Schüth, F. Kleitz, *Chem. Commun.* **2006**, 1203–1205.
[14] K. Kinoshita, *Carbon: Electrochemical and Physicochemical Properties*, John Wiley & Sons, New York, **1988**.
[15] a) M. Kruk, M. Jaroniec, C. H. Ko, R. Ryoo, *Chem. Mater.* **2000**, *12*, 1961–1968; b) S. H. Joo, R. Ryoo, M. Kruk, M. Jaroniec, *J. Phys. Chem. B* **2002**, *106*, 4640–4646; c) M. Kaneda, T. Tsubakiyama, A. Carlsson, Y. Sakamoto, T. Ohsuna, O. Terasaki, *J. Phys. Chem. B* **2002**, *106*, 1256–1266.
[16] J. Roggenbuck, M. Tiemann, *J. Am. Chem. Soc.* **2005**, *127*, 1096–1097.
[17] R. K. Iler, *The Chemistry of Silica: Solubility, Polymerization, Colloid and Surface Properties and Biochemistry*, Wiley, New York, **1979**.
[18] C. J. McDonald, M. J. Devon, *Adv. Colloid Interface Sci.* **2002**, *99*, 181–213.
[19] A. Dong, N. Ren, Y. Tang, Y. Wang, Y. Zhang, W. Hua, Z. Gao, *J. Am. Chem. Soc.* **2003**, *125*, 4976–4977.
[20] Y. Xia, R. Mokaya, *J. Mater. Chem.* **2005**, *15*, 3126–3131.
[21] A.-H. Lu, W. Schmidt, N. Matoussevitch, H. Bönnemann, B. Spliethoff, B. Tesche, E. Bill, W. Kiefer, F. Schüth, *Angew. Chem. Int. Ed.* **2004**, *43*, 4303–4306.
[22] F. Schüth, *Angew. Chem. Int. Ed.* **2003**, *42*, 3604–3622.
[23] J. Lee, S. Jin, Y. Hwang, J.-G. Park, H. M. Park, T. Hyeon, *Carbon* **2005**, *43*, 2536–2543.
[24] J. Lee, D. Lee, E. Oh, J. Kim, Y.-P. Kim, S. Jin, H.-S. Kim, Y. Hwang, J. H. Kwak, J.-G. Park, C. H. Shin, J. Kim, T. Hyeon, *Angew. Chem. Int. Ed.* **2005**, *44*, 7427–7432.
[25] H. Yang, D. Zhao, *J. Mater. Chem.* **2005**, *15*, 1217–1231.
[26] S. I. Nikitenko, Y. Koltypin, O. Palchik, I. Felner, X. N. Xu, A. Gedanken, *Angew. Chem. Int. Ed.* **2001**, *40*, 4447–4449.
[27] Z. Sun, H. Yuan, Z. Liu, B. Han, X. Zhang, *Adv. Mater.* **2005**, *17*, 2993–2997.

Received: February 15, 2007
Published Online: June 29, 2007

